Ground Vehicle Navigation Based on the Skylight Polarization

Guillaume COURTIER
French-German Research Institute of Saint-Louis (ISL)
IRIMAS UR 7499
Université de Haute-Alsace
Saint-Louis, France
guillaume.courtier@uha.fr

Pierre-Jean LAPRAY
IRIMAS UR 7499
Université de Haute-Alsace
Mulhouse, France
pierre-jean.lapray@uha.fr

Ronan ADAM
French-German Research Institute of Saint-Louis (ISL)
Saint-Louis, France
ronan.adam@isl.eu

Sébastien CHANGEY
French-German Research Institute of Saint-Louis (ISL)
Saint-Louis, France
sebastien.changey@isl.eu

Jean-Philippe LAUFFENBURGER
IRIMAS UR 7499
Université de Haute-Alsace
Mulhouse, France
jean-philippe.lauffenburger@uha.fr

***Abstract*—Autonomous or unmanned ground vehicles can take advantage of camera-based navigation systems. These navigation systems mainly rely on standard radiometric cameras. The use of polarization information, such as captured by a polarization filter array camera, is a potential extension to capture multimodal information efficiently. In this communication, we propose a navigation method that relies exclusively on Stokes images reconstructed from polarization camera data. For this purpose, an image processing pipeline is employed to estimate the heading of a vehicle. To assess the method, an acquisition card has been built and coupled with two moving platforms: a rotary stage and a moving ground vehicle. The results show that, in a dynamic car experiment, the root mean square error of the orientation is 4.29° as compared to a Global Positioning System/Inertial Navigation System.**

***Index Terms*—Polarization vision, Polarization cameras, Image understanding, Navigation, Ground vehicle**

I. Introduction

The scattering of sunlight by the sky atmosphere generates a specific polarization pattern [1], [2]. This pattern depends on the sun position relative to an observer, and can thus be used for navigation. According to the literature, the Vikings may have used the polarization skylight to navigate across the oceans, using what they called the "sunstone" which acted as a linear polarizer [3], [4]. In addition, various species, such as the North African desert ant or the mantis shrimp, are able to detect the skylight polarization features which allows them to find their way in the environment [5]–[7].

Camera-based navigation has become extensively employed, including in unmanned ground vehicles (UGVs) and autonomous vehicle [8], [9]. Existing navigation solutions are predominantly relying on conventional radiometric cameras which capture intensity signals. The use of a polarization camera is a potential improvement [6], [10], but such a system is often costly, complex, or inaccurate, e.g., a quad-camera setup with polarizers in front of each camera [11], which generates misaligned data. Other existing solutions use a camera coupled with a rotated polarizer to get different polarization states by sequential scanning [12], but produces artifacts in case of moving object/camera.

Thanks to technological advances and new types of low-cost sensors, it is now possible to quickly capture linear polarization information. The Polarization Filter Arrays (PFA) sensor is one of such devices, where a commercialized instance is the SONY IMX250 MZR [13]. In addition to being relatively inexpensive, it has the advantage of capturing four linear polarization states in a single shot, which can benefit to video applications requiring acquisition of both modalities in non-static scenes.

In this communication, we propose a compass system based exclusively on polarimetric images (i.e. Stokes images). This can overcome some disadvantages of existing solutions mentioned above. To this purpose, we developed a complete embedded acquisition system, along with an image processing algorithm, to estimate the heading of a vehicle. To assess the performances of the proposed technology, an acquisition card has been built and coupled with two moving platforms: a rotary stage and a ground vehicle. A Global Positioning System/Inertial Navigation System (GPS/INS) provides reference data for evaluation.

The paper is organized as follows: we present the imaging model and navigation method in Section II. Then, Section III describes the acquisition module and electronic cards built for

This work is also supported by the ANR JCJC SPIASI project, grant ANR-18-CE10-0005 of the French Agence Nationale de la Recherche.

capturing polarization videos, as well as their integration into the two moving platforms. Results of the acquisition campaign are reported in Section IV, before to conclude in Section V.

II. Modeling

A. Rayleigh Scattering Model

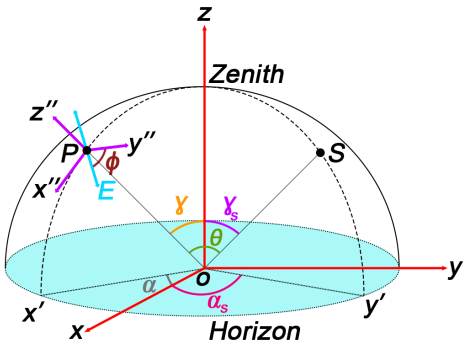

Fig. 1: Skylight polarization represented geometrically on the celestial sphere in a local frame using the E-vector with γ: zenith angle, α: azimuth angle, ϕ: polarization angle, θ: scattering angle, S: Sun position.

Rayleigh scattering is an approximation of the Mie theory [14], which is only applicable to molecules and particles with dimensions much smaller than the wavelength. Due to Rayleigh scattering by atmospheric gas molecules, the skylight has a distinct polarization pattern. It appears that skylight polarization is related to the position of the sun as well as the direction of observation. This is described by a mathematical model [1], [2] from which a spatial mapping of the angle of linear polarization (AoLP), i.e. the major axis angle of the ellipse described by the electric field, can be obtained at any daytime.

The geometrical representation involved in the Rayleigh scattering model are depicted in Fig. 1:

- The point O represents the camera. Its main axis is oriented towards the zenith and along the frame $OXYZ$.
- $OX^{'}Y^{'}Z$ is the meridian frame.
- P is the direction of observation in the celestial sphere, γ and α represent respectively the zenith angle and the azimuthal angle.
- S is the sun position in the celestial sphere, defined by γ_s/α_s the zenith/azimuth angles.
- The scattering angle is written θ.
- ϕ is the polarization angle of the scattered light given by its electric field vector $\overrightarrow{E}$ in the incident ray frame $OX^{''}Y^{''}Z^{''}$.

According to Rayleigh scattering model, $\overrightarrow{E}$ is perpendicular to the scattering plane (OPS), so that the sun vector $\overrightarrow{OS}$ is perpendicular to all polarization directions $\overrightarrow{E}$.

From Fig. 1, we define the AoLP by ϕ and the DoLP by ρ as [15], [16]:

$$\phi = tan^{-1}\left(\frac{sin(\alpha-\alpha_s)sin(\gamma_s)}{cos(\gamma_s)sin(\gamma)-sin(\gamma_s)cos(\gamma)cos(\alpha-\alpha_s)}\right), \quad (1)$$

$$\rho = \frac{1-cos^2(\theta)}{1+cos^2(\theta)}. \quad (2)$$

According to (1), we can see that the AoLP is calculated with a $180°$ indeterminacy, similarly when $\alpha = \alpha_s$ and $\alpha = \alpha_s + 180°$, the AoLP is equal to $0°$. In addition, from (2), DoLP is equal to 0 and 1 when $\theta = 0°$ and $\theta = 90°$ respectively.

B. Imaging Model

Stokes parameters allow a complete mathematical description of the polarization state of the light with a four components vector $\mathbf{S}$ [17]:

$$\mathbf{S} = \begin{bmatrix} S_0 \\ S_1 \\ S_2 \\ S_3 \end{bmatrix}, \quad (3)$$

where S_0 is the total light intensity, S_1 is the intensity difference between $0°$ and $90°$ polarizers, S_2 is the intensity difference between $45°$ and $135°$ polarizers, and S_3 is the difference between right and left circular polarization. As circular polarization is very rarely represented in nature, S_3 is assumed to be zero in this work.

It is necessary to use a measurement device called a polarimeter to determine the Stokes parameters. A measured intensity I is captured relatively to a polarization filter oriented at an angle φ. The intensity results from a linear combination of the incident Stokes vector $\mathbf{S}$ and the analyzer vector $\mathbf{A}$ (which characterizes the polarizer characteristics, i.e. the transmission, the orientation, and the extinction ratio) as follows:

$$I = \mathbf{AS}. \quad (4)$$

To estimate the first three components of the Stokes vector, several measurements are needed. Thus, M measured intensities I_φ are captured relatively to M polarization filter orientations φ. In this work, we use a PFA camera that has $M = 4$ polarizer orientations $\varphi \in \{0°, 45°, 90°, 135°\}$ (see Fig. 3). The SONY IMX250 MZR sensor can be assumed to be a near to ideal polarimeter when using conventional camera lens parameters (relatively high focal length and low aperture) [18]. This leads to a specific analyser matrix $\mathbf{W} = \mathbf{W_{ideal}}$, composed by a group of four analysis vectors [19]. Equation (4) can be rewritten as:

$$\mathbf{I} = \begin{bmatrix} I_0 \\ I_{45} \\ I_{90} \\ I_{135} \end{bmatrix} = \mathbf{W_{ideal}S} = \frac{1}{2}\begin{bmatrix} 1 & 1 & 0 \\ 1 & 0 & 1 \\ 1 & -1 & 0 \\ 1 & 0 & -1 \end{bmatrix}\begin{bmatrix} S_0 \\ S_1 \\ S_2 \end{bmatrix}. \quad (5)$$

The Stokes vector $\hat{\mathbf{S}}$ can be estimated by:

$$\hat{\mathbf{S}} = \mathbf{W}^{+}_{\mathbf{ideal}}\mathbf{I}, \quad (6)$$

where the subscript $+$ means the pseudo-inverse estimator.

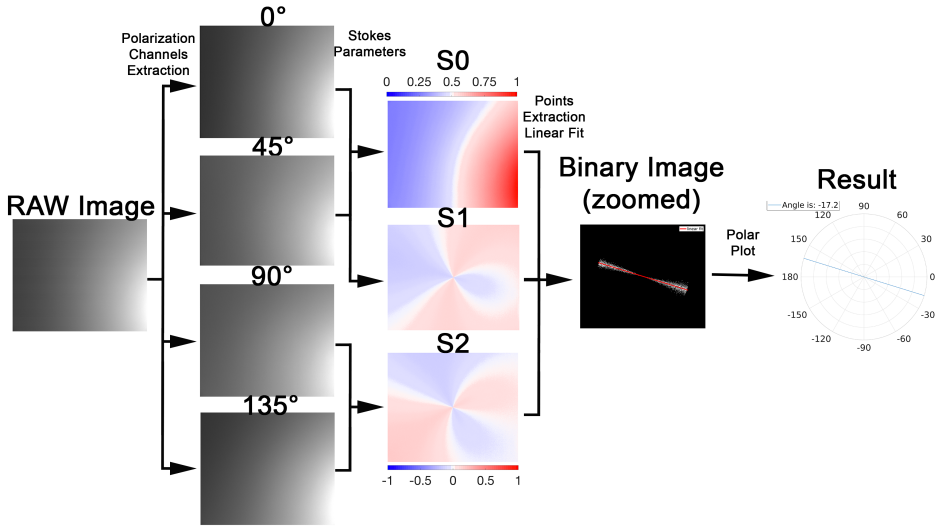

Fig. 2: Visualization of the imaging pipeline steps used in this article for heading estimation. The RAW image is captured from the PFA camera (SONY IMX250 MZR).

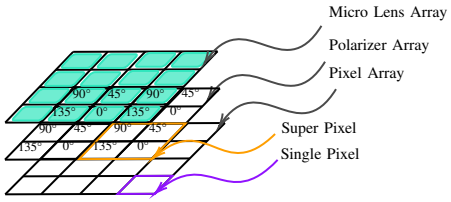

Fig. 3: Architecture of the PFA camera used as a polarimeter in this work. The polarizer arrangement is specific to the Sony IMX250 MZR sensor.

The AoLP can then be defined from Stokes parameters as follows:

$$\phi = \frac{1}{2}\tan^{-1}\left(\frac{S_2}{S_1}\right). \tag{7}$$

The DoLP is computed as follows:

$$\rho = \frac{\sqrt{S_1^2 + S_2^2}}{S_0}. \tag{8}$$

C. Navigation Method

As explained in Section II-A, all the points in the celestial sphere defined by an azimuthal angle corresponding to the direction of the sun ($\alpha = \alpha_s$) have an AoLP of $0°/180°$. Consequently, in order to estimate the heading of a vehicle relative to the sun from an image of the skylight polarization, we must find in the captured image, the line corresponding to $0°/180°$. According to (7), it can also equivalently be determined by the following conditions: $S_1 < 0$ and $S_2 = 0$. In the context of an embedded system with real-time capability, it would be better to use directly S_0, S_1, S_2 as an estimator, instead of computing the AoLP/DoLP. This eliminates the need of computing non-linear functions which are difficult to implement in hardware (such as in an FPGA), and thus saving computation time. The $180°$ ambiguity could be solved as S_0 maximum corresponds to the sun position.

We define a practical imaging pipeline (see Fig. 2), that is a modified version of published pipeline [20]. The imaging pipeline consists of several steps:

1) Sub-sampling of the captured raw mosaiced PFA image to get four polarization state images ($\mathbf{I}_0$, $\mathbf{I}_{45}$, $\mathbf{I}_{90}$, and $\mathbf{I}_{135}$ images).
2) Stokes vector image reconstruction using (6). It is necessary to make a change of frame on S_1 and S_2 to pass from the incident ray frame to the meridian frame with the following rotation matrix:

$$\boldsymbol{R} = \begin{bmatrix} cos(\alpha) & sin(\alpha) \\ -sin(\alpha) & cos(\alpha) \end{bmatrix}. \tag{9}$$

The azimuthal angle α is expressed as follows:

$$\alpha = \tan^{-1}\left(\frac{y}{x}\right), \tag{10}$$

where x and y are the pixels coordinates.
3) Thresholding operation to get a binary image $\mathbf{BW}$ from S_0, S_1, and S_2 as follows:

$$BW(x,y) = \begin{cases} 1 & if\ S_1(x,y) < 0\ and\ |S_2(x,y)| < T, \\ 0 & otherwise, \end{cases} \tag{11}$$

where T is a threshold for the tolerance (arbitrarily set at $T = 0.01$). An example of a binary image is shown in Fig. 2. We have experienced that some spatially isolated pixels in $\boldsymbol{BW}$ correspond to false positives, and are directly related to obstacles (trees, building, etc.). By assuming that the line area of detected pixels should only contain adjacent positives, we apply a median filtering to $\boldsymbol{BW}$ to remove false positives. This obstruction issue has already been tackle in the literature, but with a more

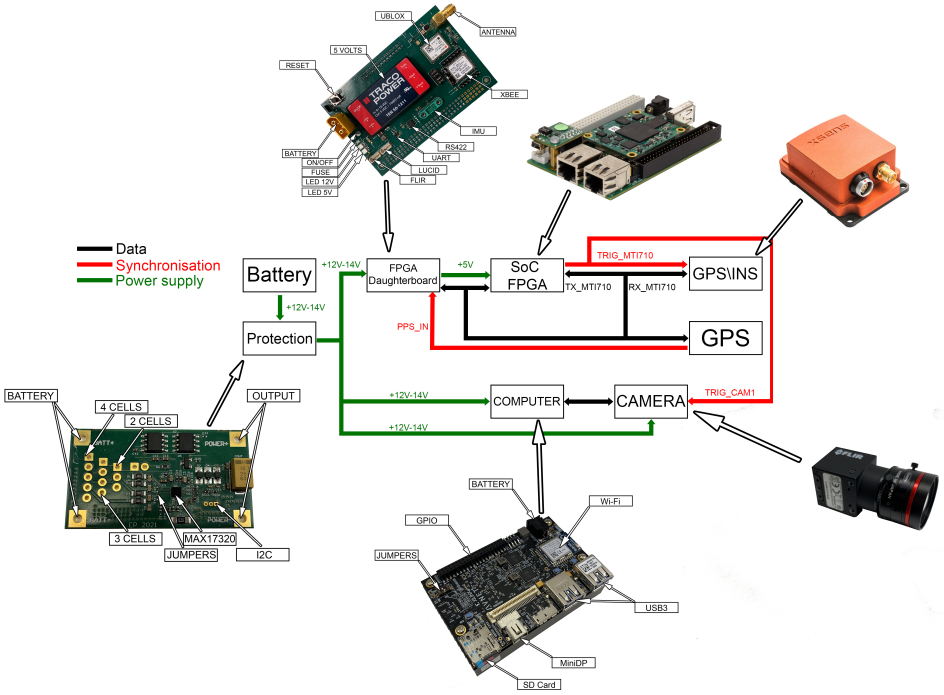

Fig. 4: Hardware architecture of the image acquisition and electronic cards used in the experiment.

computationally expensive method [21], i.e. using the gradient of the degree of the polarization.

4) Least squares regression to find a straight line passing through the pixels with a level of 1 (white) in the $\boldsymbol{BW}$ image.

Let's define the equation:

$$\mathbf{Y} = \begin{bmatrix} y_1 \\ \vdots \\ y_i \\ \vdots \\ y_n \end{bmatrix} = \mathbf{XA} = \begin{bmatrix} x_1 & 1 \\ \vdots & \vdots \\ x_i & 1 \\ \vdots & \vdots \\ x_n & 1 \end{bmatrix} \begin{bmatrix} a \\ b \end{bmatrix}, \tag{12}$$

where $(x_i, y_i)_{1 \leq i \leq n}$ are the coordinates of the n^{th} extracted pixels labelled with $BW = 1$, and $(a, b) \in \mathbb{R}^2$ are the parameters of the straight line to be estimated. They are computed using the following equation:

$$\mathbf{A} = \begin{pmatrix} a \\ b \end{pmatrix} = \mathbf{X}^{+}\mathbf{Y}. \tag{13}$$

Finally, the estimation of the direction of the sun relative to the vehicle frame is given by:

$$\theta = \tan^{-1}(a). \tag{14}$$

Obviously, the $\boldsymbol{X}$ matrix in (12) cannot be inverted when the line to estimate is aligned with the y-axis. To resolve this issue, $(x_i)_{1 \leq i \leq n}$ and $(y_i)_{1 \leq i \leq n}$ are swapped during the estimation process according to:

- if $\sigma_{y_i} \geq \sigma_{x_i}$: use (12)
- if $\sigma_{y_i} < \sigma_{x_i}$: swap $(x_i)_{1 \leq i \leq n}$ and $(y_i)_{1 \leq i \leq n}$ in (12)

III. Experiment

To verify the efficiency of our imaging pipeline and navigation algorithm, we built an experiment with complete portable acquisition system to generate both image data and reference data. We embedded it into two different platforms and carried out several acquisition campaigns.

A. Camera

The PFA camera is the Flir BlackFly S USB3 BFS-U3-51S5P-C with a SONY IMX250 MZR sensor (see Fig. 3). The imaging lens is a Kowa LM8JC5MC, with a focal length of $8\,mm$ and an aperture of $F2.8$ which provides a somewhat acceptable balance between the field of view, light output, and lens distortion.

B. Electronic Cards

The acquisition is ensured by a remote controllable embedded system, made up of two SoC FPGA boards (Avnet Ultra96-V2 and Trenz TE0706 with SoC module TE0715). The first board is in charge of the camera acquisition, and the second board is responsible for synchronization and acquisition of the reference data of GPS/INS. The functional diagram of the system is presented in Fig. 4.

C. Platforms & Data Acquisition

The acquisition system was embedded into those two test platforms:

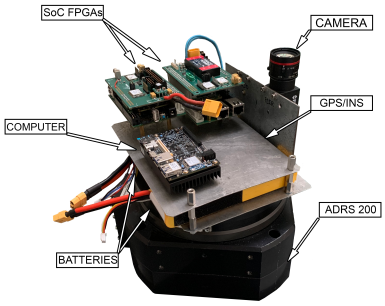

(a)

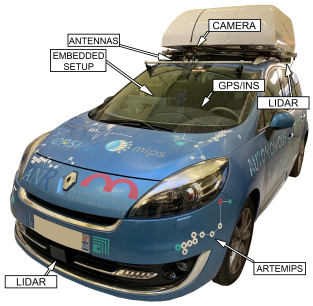

(b)

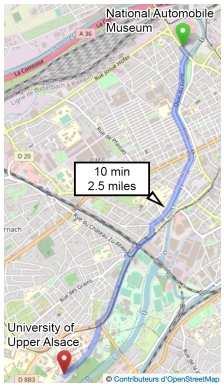

(c)

Fig. 5: The two test platforms used for experiments. (a) Rotary bench coupled with the acquisition cards described in Section III. (b) ARTEMIPS (a car prototype [22]) coupled with the acquisition cards. (c) Experience itinerary for the experiment with ARTEMIPS.

1) Rotary Bench: A rotary setup (see Fig. 5a) is used to assess the precision of the proposed solution in a static frame. The objectives of this set up is to verify the navigation algorithm and to receive feedback on how well it performs in a controlled environment. A mechanical-bearing direct-drive rotary stage (Aerotech ADRS 200, accuracy: $0.002°$ on the calibrated encoder) makes up the device. The included encoder serves as a reference to get the heading. The camera is mounted on a $90°$ metal L-shape.

The acquisition took place in clear weather condition and without clouds. The rotary bench is progressively rotated from $0°$ to $360°$ at a rate of $0.3\,Hz$, the angular displacement computed with the camera is compared to the bench feedback (see Fig. 6).

2) ARTEMIPS: We embedded the system on a ground vehicle named ARTEMIPS (see Fig. 5) (Autonomous Real-Time Experimental platform of IRIMAS) which serves as a test and validation vehicle [22]. It was equipped with the polarized camera as well as an GPS/INS (Xsens MTi-G-710, accuracy: $0.8°$ RMS on the heading) mounted in the vehicle at the center of gravity. The GPS/INS is used as reference data.

The acquisition campaign took place in downtown Mulhouse, France on 03/28/2022 at 12:14 PM. The path was 2.5 miles long and took 10 minutes (see Fig. 5c). The sky was fairly clear with only a few clouds and the weather was good. The acquisition environment includes trees, traffic, pedestrians, tunnels, and buildings.

IV. Results and Analysis

A. Rotary Bench

Fig. 6 shows the rotary bench estimation results. We see that the heading computed from the polarization information and the rotary bench encoder are relatively closed. The heading is computed from $0°$ to $180°$ due to the $180°$ indeterminacy on the Sun position. We obtained a Root Mean Square Error (RMSE) of $1.83°$ for the camera compared to the rotary bench encoder (see TABLE I). A minimum and maximum errors of $-1.90°$ and $4.10°$ is observed respectively. These errors experimentally characterize the performance of our heading estimation system.

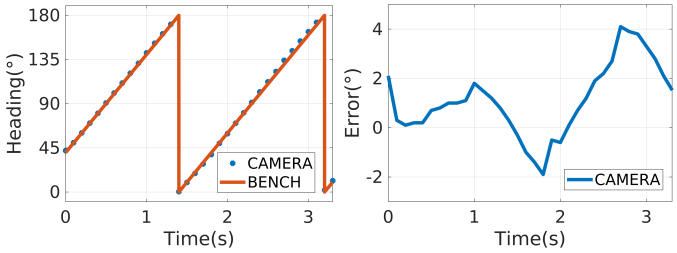

(a) (b)

Fig. 6: Rotary bench experiment results. (a) Estimation of the heading by the camera. (b) Heading errors with respect to the rotary bench encoder.

B. ARTEMIPS

The comparison between the heading delivered by the Xsens MTi-G-710 and the proposed method is displayed in Fig. 7. The results show that the estimation of the heading is estimated with a RMSE of $4.29°$ with respect to the GPS/INS for the total itinerary.

From Fig. 7a, it can be seen that the behaviors of the plots are very consistent. From the zoom area in Fig. 7a, it is clear that the heading estimation of our solution can follow rapid changes in orientation/heading (like at $time = 70\,s$). Nevertheless, we notice that there is a near-to-constant negative offset all along the itinerary between the camera estimation and the GPS/INS data. This offset can have a great influence on the RMSE value computed in TABLE I, and thus needs to be investigated in the future.

The results should be put into perspective, given that our GPS/INS system does not have a high precision for heading estimation purpose ($0.8°$). This could explain the offset we have. The use of a better reference device, like a precise North-finding system as in [21], would probably make it possible to refine the evaluation of the method relatively to better reference data.

By looking at Fig. 7b, we can see that there are some glitches which appears suddenly with apparently no reason

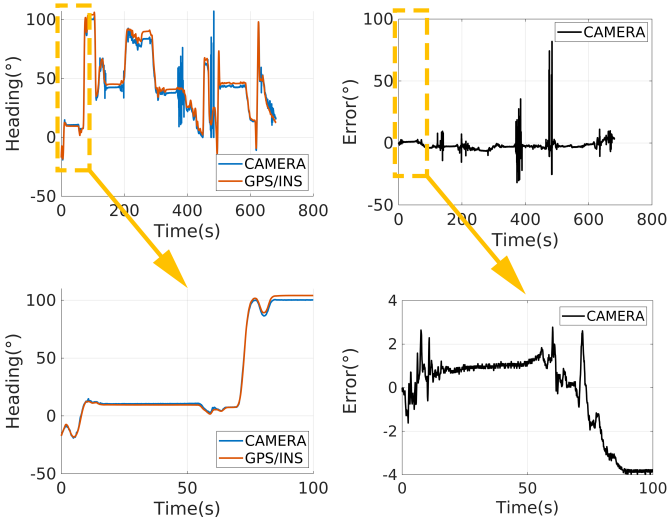

(a) (b)

Fig. 7: ARTEMIPS experiment results. (a) Estimation of the heading by the camera compared to the GPS/INS which is used as reference. (b) Computation of the errors of the camera compared to the GPS/INS. The zoomed area represents a portion of the itinerary without any sky obstruction by environment.

(steep heading transition like at $time = 400\,s$). This can be explained by obstructions of the sky by objects like trees, tunnels, or buildings (see an example in Fig. 8). According to this last figure, it can be seen that a lot of noise is adding to the image because of the presence of trees in the scene; moreover, some depolarization is also added by the building, influencing the BW image and therefore the heading estimated which is shifted by about ten degrees. On the other hand, as our heading estimation is absolute, an error on a frame does not bring accumulation of errors unlike visual odometry or drift in time as rate gyros. The zoomed area in Fig. 7 is a portion of the itinerary without any disturbing element. We obtain a RMSE of $1.86°$ (see TABLE I), which is in accordance with the results found with the rotary bench. Compared to the literature, such as the work of Fan *et al.*, our system is not as accurate as theirs (they have an RMSE of $0.81°$) but we do not do any data fusion. Moreover, as explained above, the heading accuracy of the GPS/INS is only $0.8°$. Our system is based only on the calculation of heading by the camera, which can be disturbed by environmental factors.

Finally, from our understanding, the obtained heading error is a combination of the intrinsic errors of your system, environmental obstructions of the sky generating false positives in the BW image and of the performance of the GPS/INS.

V. Conclusion

In conclusion, we propose a compass system that is entirely based on polarimetric images. To that end, we created a complete embedded acquisition system as well as an image processing algorithm to estimate the heading of a vehicle.

TABLE I: Error statistics for the two experiments. The zoomed column corresponds to the errors of the zoomed area in Fig. 7.

	Rotary Bench	***ARTEMIPS (Total)***	***ARTEMIPS (Zoomed)***
$\overline{E}$	$1.11°$	$-2.06°$	$-0.24°$
$RMSE$	$1.83°$	$4.29°$	$1.88°$
Min	$-1.90°$	$-31.88°$	$-3.98°$
Max	$4.10°$	$81.85°$	$2.78°$
σ	$1.47°$	$3.77°$	$1.86°$

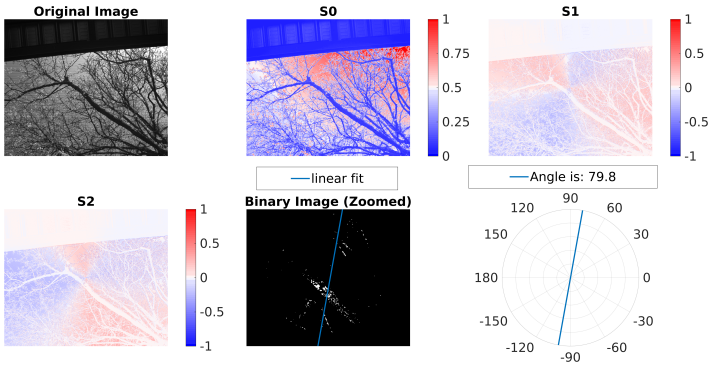

Fig. 8: Example of the environmental impact on the data (tree, building and tunnel).

To evaluate the performance of the proposed technology, an acquisition card was built and embedded in two moving platforms: a rotary stage and a ground vehicle. A GPS/INS provided the reference data. An error of few degrees has been quantified between the reference and the estimated headings. These errors are a combination of the intrinsic errors of your system, environmental obstructions and of the performance of the GPS/INS used as a reference. The advantages of our system are that it is based on a low cost polarimetric sensor, that the heading estimation method is absolute and that there is no need for other sensors. The main drawback is that it is sensitive to environmental factors.

As a future work, we want to study the impact of the configuration of the imaging system, e.g. varying the spectral selectivity of the camera, as well as the parameters of the imaging lens (focal length, aperture). The final perspective is to implement the system in an Unmanned Aerial Vehicle (UAV) in order to estimate the attitude and thus to pass from a 2D environment to a 3D environment.

Acknowledgment

The authors would like to thank Emmanuel Pecheur, Jonathan Braun and Frédéric Walter for their help in the development of the acquisition system as well as for their help during the tests. We also wish to thank the IRIMAS laboratory and more precisely the MIAM team with notably Michel Basset, Jonathan Ledy and Thomas Josso-Laurain for the loan of the ARTEMIPS vehicle and their precise help during

the tests with it. Finally, we thank the National Automobile Museum of Mulhouse for having borrowed their test track.

REFERENCES

[1] J. Strutt, "Investigation of the disturbance produced by a spherical obstacle on the waves of sound," *Proceedings of the London Mathematical Society*, vol. 1, no. 1, pp. 253–283, 1871.

[2] V. Twersky, "Rayleigh scattering," *Applied Optics*, vol. 3, no. 10, pp. 1150–1162, 1964.

[3] J. Marchant, "Did vikings navigate by polarized light?" 2011.

[4] G. Horváth, A. Barta, I. Pomozi, B. Suhai, R. Hegedüs, S. Åkesson, B. Meyer-Rochow, and R. Wehner, "On the trail of vikings with polarized skylight: experimental study of the atmospheric optical prerequisites allowing polarimetric navigation by viking seafarers," *Philosophical Transactions of the Royal Society B: Biological Sciences*, vol. 366, no. 1565, pp. 772–782, 2011.

[5] L. Cartron, A.-S. Darmaillacq, C. Jozet-Alves, N. Shashar, and L. Dickel, "Cuttlefish rely on both polarized light and landmarks for orientation," *Animal cognition*, vol. 15, no. 4, pp. 591–596, 2012.

[6] J. Dupeyroux, J. Diperi, M. Boyron, S. Viollet, and J. Serres, "A novel insect-inspired optical compass sensor for a hexapod walking robot," in *2017 IEEE/RSJ International Conference on Intelligent Robots and Systems (IROS)*. IEEE, 2017, Conference Proceedings, pp. 3439–3445.

[7] G. Horváth and R. Wehner, "Skylight polarization as perceived by desert ants and measured by video polarimetry," *Journal of Comparative Physiology A*, vol. 184, no. 1, pp. 1–7, 1999.

[8] J. Gaspar, N. Winters, and J. Santos-Victor, "Vision-based navigation and environmental representations with an omnidirectional camera," *IEEE Transactions on robotics and automation*, vol. 16, no. 6, pp. 890–898, 2000.

[9] M. Rebert, D. Monnin, S. Bazeille, and C. Cudel, "Parallax beam: a vision-based motion estimation method robust to nearly planar scenes," *Journal of Electronic Imaging*, vol. 28, no. 2, p. 023030, 2019.

[10] R. Blin, S. Ainouz, S. Canu, and F. Meriaudeau, "Multimodal polarimetric and color fusion for road scene analysis in adverse weather conditions," in *2021 IEEE International Conference on Image Processing (ICIP)*, 2021, pp. 3338–3342.

[11] C. Fan, X. Hu, X. He, L. Zhang, and Y. Wang, "Multicamera polarized vision for the orientation with the skylight polarization patterns," *Optical Engineering*, vol. 57, no. 4, p. 043101, 2018.

[12] J. Dupeyroux, S. Viollet, and J. R. Serres, "Polarized skylight-based heading measurements: a bio-inspired approach," *Journal of the Royal Society Interface*, vol. 16, no. 150, p. 20180878, 2019.

[13] Sony, "Polarization image sensor," Polarsens, Report, 2018.

[14] G. Mie, "Beiträge zur optik trüber medien, speziell kolloidaler metallösungen," *Annalen der Physik*, vol. 330, no. 3, pp. 377–445, 1908. [Online]. Available: https://onlinelibrary.wiley.com/doi/abs/10.1002/andp.19083300302

[15] Y. Wang, X. Hu, J. Lian, L. Zhang, Z. Xian, and T. Ma, "Design of a device for sky light polarization measurements," *Sensors*, vol. 14, no. 8, pp. 14 916–14 931, 2014.

[16] Y. Wang, X. Hu, J. Lian, L. Zhang, and X. He, "Bionic orientation and visual enhancement with a novel polarization camera," *IEEE Sensors Journal*, vol. 17, no. 5, pp. 1316–1324, 2017.

[17] G. G. Stokes, "On the composition and resolution of streams of polarized light from different sources," *Transactions of the Cambridge Philosophical Society*, vol. 9, p. 399, 1851.

[18] C. Lane, D. Rode, and T. Rösgen, "Calibration of a polarization image sensor and investigation of influencing factors," *Appl. Opt.*, vol. 61, no. 6, pp. C37–C45, Feb 2022. [Online]. Available: http://www.osapublishing.org/ao/abstract.cfm?URI=ao-61-6-C37

[19] Z. Chen, X. Wang, and R. Liang, "Calibration method of microgrid polarimeters with image interpolation," *Appl. Opt.*, vol. 54, no. 5, pp. 995–1001, Feb 2015. [Online]. Available: https://opg.optica.org/ao/abstract.cfm?URI=ao-54-5-995

[20] G. Courtier, R. Adam, P.-J. Lapray, E. Pecheur, S. Changey, and J.-P. Lauffenburger, "Image-based navigation system using skylight polarization for an unmanned ground vehicle," in *Unmanned Systems Technology XXIV*, H. G. Nguyen, P. L. Muench, and B. K. Skibba, Eds., vol. 12124, International Society for Optics and Photonics. SPIE, 2022, p. 121240H. [Online]. Available: https://doi.org/10.1117/12.2616833

[21] C. Fan, X. Hu, X. He, L. Zhang, and J. Lian, "Integrated polarized skylight sensor and mimu with a metric map for urban ground navigation," *IEEE Sensors Journal*, vol. 18, no. 4, pp. 1714–1722, 2018.

[22] H. Laghmara, M.-T. Boudali, T. Laurain, J. Ledy, R. Orjuela, J.-P. Lauffenburger, and M. Basset, "Obstacle avoidance, path planning and control for autonomous vehicles," in *2019 IEEE Intelligent Vehicles Symposium (IV)*, 2019, pp. 529–534.